Simulation of Dislocation Accumulation in ULSI Cells with STI Structure

Tetsuya Ohashi [a], Michihiro Sato [a], Takuya Maruizumi [b], Isao Kitagawa [b]

[a] Kitami Institute of Technology,
Koencho 165, Kitami, Hokkaido, 090-8507, Japan
Phone : +81-157-26-9215, Fax : +81-157-23-9375, E-mail : sato@newton.mech.kitami-it.ac.jp

[b] Advanced Research Laboratory, Hitachi, Ltd.,
Higashi-koigakubo, Kokubunji, Tokyo, 185-8601, Japan

Abstract

The periodic structure of the shallow trench isolation (STI) type ULSI cells is generally used for the latest semiconductor device structure. However, dislocations sometimes accumulate in the electron channel when the device size becomes small, and they have an enormous effect on the electronic state and obstruct the device from normal operation. In this paper, we numerically model the periodic structure of the STI type ULSI cells, and analyze the plastic slip that takes place during the oxidation process of oxide film area. The slip deformation is analyzed by a crystal plasticity analysis cord, which has been developed on the basis of finite element technique, and we evaluate the accumulation of dislocations that accompany plastic slip. The results show stress concentrations at the shoulder part of the device area and the bottom corners of the trench for the device isolation, and high stresses at these area cause plastic slip and dislocation accumulation. The direction of these dislocation lines are shown to be mostly parallel to the trench direction and dislocations are approximately 60° mixed type.

Key Words : ULSI, Shallow trench isolation, dislocation, crystal plasticity analysis, finite element method

1. Introduction

High-density memories and high-speed CPUs are usually realized by a reduction of the size of semiconductor cells in LSIs. Representative length scale of ULSI cells is going to be at a nano-meter order, and the atomic level defects, such as uneven oxidation film or lattice defect generation are becoming more and more important. Among them, dislocations which often appear near hetero-interfaces and accumulate in the electron channel have an enormous effect on the electronic state of the device, increase the signal delay and obstruct devices from normal operation. Therefore, the evaluation and control of dislocations is crucial not only for the design of cell structure, but also for the design of process through which ULSI chips are produced. The periodic structure of the shallow trench isolation (STI) type ULSI cells are generally adopted as the latest semiconductor device structure. A lot of investigations have been made [1]-[6] on this type of structure, but detailed aspects on dislocations and their density distribution in the cells are not fully understood.

In the present study, we analyze plastic slip that take place in the STI structure during the oxidation process of oxide film area, and evaluate the accumulation of dislocations that accompany plastic slip, using a numerical continuum mechanics technique of crystal plasticity analysis. Structure of dislocations are visualized from the numerical

results, and density distribution and crystallographic character of dislocations are discussed.

2. Model for numerical analysis

Fig.1 schematically shows the periodic structure of the STI type ULSI cells. Our numerical model for the analysis is one unit of the periodic structure; the part between the dotted lines in Fig.1. Fig.2 shows the analysis model. We employ three different sets of dimensions for the model (Table 1). Here, L_g is the gate length of the device. The models are divided into finite elements and the type of the elements is the composite element with eight nodes. The numbers of nodes and elements in a model are 11956 and 8640, respectively. The device consists of the volumes ① to ⑥, as shown in Fig.2. Volumes ① to ③ correspond to buried oxide, gate electrode and source/drain electrodes, respectively, and for simplicity their materials are assumed to be SiO2. Volumes ④ and ⑤ are the film region where dilatational transformation takes place due to oxidation, and volume ⑥ represents the Si substrate. Crystal orientation of the model is also shown in Fig.2. The normal of Si substrate (the Y axis) corresponds to the [100] direction and trench direction of STI structure corresponds to the [011] direction.

Fig. 1
Fig. 2
Table 1

3. Crystal plasticity analysis.

Let us suppose that plastic deformation in the volumes ①, ②, ③ and ⑥ of crystalline structure take place by slip and the plastic slip accompanies movement and

accumulation of dislocations. Volumes ④ and ⑤ are supposed to deform only elastically, on which we discuss later. The plastic slip occurs on (111) slip plane in [110] slip direction and there are 12 combinations of slip plane and slip direction, which define the 12 slip systems. Dislocations which accumulate after plastic slip are categorized into two kinds; statistically stored dislocations (SS dislocations) and geometrically necessary dislocations (GN dislocations). Accumulation of the geometrically necessary dislocations is studied in this paper. The geometrically necessary dislocations accompany to the spatial gradient of plastic shear strain on slip systems. Ashby introduced the one-dimensional concept of geometrically necessary dislocations as follows [7];

$$\rho_G \cdot \tilde{b} = -\frac{\partial \gamma}{\partial \xi} \quad , \tag{1}$$

where, ρ_G is the density of the geometrically necessary dislocations. γ, $\tilde{b}$ and ξ are the plastic shear strain, the magnitude of the Burgers vector, and the direction parallel to the slip direction on the slip plane, respectively. In three dimensional space, the densities of geometrically necessary dislocations are given for the edge and the screw components [8];

$$\rho^{(n)}_{G,edge} \cdot \tilde{b} = -\frac{\partial \gamma^{(n)}}{\partial \xi^{(n)}} \quad , \tag{2}$$

$$\rho^{(n)}_{G,screw} \cdot \tilde{b} = \frac{\partial \gamma^{(n)}}{\partial \zeta^{(n)}} \quad , \tag{3}$$

where, superscript (*n*) denotes the slip system number. Deformation analysis is made by a software code [9] which analyzes the plastic slip on {111}<110> slip systems and evaluates stresses in microstructure. Gradient of plastic shear strain on each element is

evaluated also. The density of geometrically necessary dislocations $\|\rho_G\|$ and the characteristic angle ϕ between the line segment of GN dislocation and the Burgers' vector are given by the following eqs. [10];

$$\left\|\rho_G^{(n)}\right\| = \sqrt{(\rho_{G,edge}^{(n)})^2 + (\rho_{G,screw}^{(n)})^2} \quad , \tag{4}$$

$$\sin\phi = \frac{\rho_{G,edge}}{\|\rho_G\|} \quad , \qquad \cos\phi = \frac{\rho_{G,screw}}{\|\rho_G\|} \quad , \tag{5}$$

When ϕ is 0, the segment has positive screw character, and when $\phi = \pi/2$ the segment has positive edge character. When ϕ is between 0 and $\pi/2$, the segment has a mixed character of positive screw and edge dislocations.

We analyze the deformation of the model during a dilatation of the films ④ and ⑤, which is supposed to take place due to their oxidation. Theoretical value for the volumetric strain due to the oxidation is 100%. However, the film areas which are not free standing but buried in the ULSI cells will experience viscous flow at high temperature during the cell formation processes and stress will be reduced greatly. As far as we know, there is no available technique to evaluate the stress relaxation due to the viscous flow together with the evaluation of plastic slip in crystalline material area. In the present analysis, we assume that there is no viscous flow in the oxide films and, in place of that, we assume a very small ($\varepsilon = 3.5\times10^{-3}$) the volumetric strain. Therefore, the absolute values obtained in this analysis do not have any physical significance, although qualitative aspects, such as behavior of the dislocations and their relative relationships, give us an insight for dislocation processes at the first stage of oxidation. Table.2 shows the material data [11]-[13] used for the analysis. Table 2

Lateral surfaces of the model are constrained in the following way. We neglect the deformation in the z direction because the dimension of the STI structure in the z direction is long enough compared to those in the x and the y direction. Then, in the numerical model, the nodes on the surfaces perpendicular to the z axis are constrained to displace in the z direction. On the other hand, the nodes on the surfaces which are perpendicular to the x axis are subjected to obey a periodic boundary condition in the x direction.

4. Results and discussion

Fig.3 shows a numerical result for the density distribution of the geometrically necessary dislocations on $(111)[1\bar{1}0]$ slip system. Longer and thicker line segments represent higher density of dislocations. Direction of line segments is parallel to the dislocation line. Stress concentrates at the shoulder part of the device and bottom corners of the trench and this causes plastic slip and dislocations accumulation at these areas. Directions of these dislocation lines are mostly parallel to the z axis and parallel to the intersection line of slip plane and the film-substrate. The characteristic angles for dislocations at these areas are approximately 60° and –120°. In the model 1, dislocations accumulate only at the right shoulder part of the device area. In the model 2, whose width and gate length are about 2/3 of the model 1, higher density of dislocations accumulate also at the bottom left corner of the trench. In the model 3 in which the cell dimension is reduced to 30% of model 2, dislocations with the highest densities are observed. Fig. 3

Fig.4 shows volume frequency distribution of finite elements where dislocation density is larger than 1.0×10^{14} m^{-2} . The horizontal axis is the dislocation density; the dislocation density is between 1 and 2.0×10^{14} m^{-2} in about 0.12% volume within the model 3, for example. The maximum dislocation densities in the models 1 and 2 are approximately 1.3×10^{14} m^{-2} and 3.2×10^{14} m^{-2}, respectively. In the model 3, dislocations with the density larger than 1.0×10^{15} m^{-2} accumulate in about 0.01% volume of the model. That is the reduction of the device size causes higher dislocation density and larger volume fraction is occupied by dislocations. Fig. 4

Dislocations on the $(111)[1\bar{1}0]$ slip system accumulates mainly at three areas in the device as shown in Fig.3. Fig.5 shows average dislocation densities in these three areas as a function of the gate length of the cells. In the model 1 with the longest gate length, dislocations mainly accumulate at the area B, and the dislocation densities at the areas A and C are relatively small. In the model 2, dislocation density in the area B is approximately the same with that in the model 1, while the density in the area A increases. In the model 3 with the smallest gate length in our model, dislocation densities are about 3 times larger than those in the model 2. Fig. 5

In this analysis, we observe slip deformation on 6 slip systems among 12, which are show in Table 3. Dislocation structures on slip systems 3, 4 and 6 are similar, but with some mirror symmetry, to that obtained for the slip system 1, which we showed in Figs.3-5. Dislocations on slip systems 8 and 11 were not straight but they formed half loops emerging from the edges of hetero-interfaces between the Si substrate and oxide Table 3

film and their maximum densities in the models 1,2 and 3 were about 4.5×10^{14} m^{-2} , 5.7×10^{14} m^{-2} and 1.9×10^{15} m^{-2} , respectively.

5. Conclusion

We analyzed dislocation accumulation which took place due to formation of oxide film in the periodic structure of the shallow trench isolation (STI) type ULSI cells. Character of dislocations, and their density distribution were evaluated and the results are summarized as follows;

(1) During the oxidation process, stress concentrates at the shoulder part of the device area and bottom corners of the trench and this causes generation and accumulation of dislocations at these areas.

(2) The direction of dislocation was mostly parallel to the trench direction and these dislocations were proved to be approximately 60° mixed type.

(3) When the device size was reduced and gate length became small, a higher density of dislocations accumulate, especially at the bottom corners of the trench.

Acknowledgments

This work was done under a financial support from the project of “Research and Development for Applying Advanced Computational Science and Technology (ACT-JST)” at Japan science and technology corporation (JST). Mr. Akihito Umano is also acknowledged for his elaboration on geometrical modeling during his thesis work at Kitami institute of technology.

References

[1] J.W.Sleight., C.Lin., G.J.Grula., IEEE Trans. Electron Deivces, 20(1999),248.

[2] S-H.Pyi., I-S.Yeo., D-H.Weon., Y-B.Kim., H-S.Kim., S-K.Lee., IEEE Trans. Electron Deivces, 20(1999),384.

[3] D.Ha., C.Cho., D.Shin., G-H.Koh., T-Y.Chung., K.Kim., IEEE Trans. Electron Deivces, 45(1999),940.

[4] P.Smeys., P.B.Griffin., Z.U.Rek., I.D.Wolf., K.C.Saraswat., IEEE Trans. Electron Deivces, 46(1999),1245.

[5] J-W.Lee., H-K.Kim., W-H.Lee., M-R.Oh., Y-H.Koh., IEEE Trans. Electron Deivces, 47(2000),1013.

[6] P.VanDerVoorn., D.Gan., J.P.Krusius., IEEE Trans. Electron Deivces, 47(2000),1175.

[7] Ashby, M.F., Phil.Mag., 21(1970),399.

[8] Ohashi, T., Phil. Mag. Lett., 75(1997), 51.

[9] Ohashi, T., Phil. Mag., A70(1994), 793.

[10] Ohashi, T., J. Phys. Ⅳ France, 9(1999), 279.

[11] *Semiconductors Handbook*, revised ed., edited by Semiconductors Handbook Compilation Committee (Ohm-sha Publishing, Tokyo, 1977), p. 135.

[12] *Encyclopedia for Physics and Chemistry*, 3rd ed., edited by B. Tamamushi (Iwanami Publishing, Tokyo, 1981), pp. 1068,1151.

[13] *Physical constant Handobook*, revised ed., edited by S. Iida (Asakura Publishing, Tokyo, 1979), pp. 25,124

Caption list :

Fig. 1. Schematic illustration of the periodic structure of the STI type ULSI cells. One unit of the periodic structure is used for the analysis.

Fig. 2. Model employed for the crystal plasticity analysis. Volumes ① to ③ correspond to buried oxide, gate electrode, and source/drain electrodes, respectively. Volumes ④ and ⑤ correspond to the film region where dilatational transformation take place due to oxidation, and volume ⑥ represents the Si substrate, respectively. Crystal orientation of <011>, <100> and $<01\bar{1}>$ correspond to x, y and z axis, respectively.

Fig. 3. Numerical result for dislocations which accumulate on the $(111)[1\bar{1}0]$ slip system. Longer and thicker line segments represent higher density of dislocations.

Fig. 4. Volume frequency distribution of finite elements where dislocation density is larger than 1.0×10^{14} m^{-2}. The maximum dislocation densities in the model 1, 2 and 3 are 1.3×10^{14} m^{-2}, 3.2×10^{14} m^{-2} and 1.1×10^{15} m^{-2}, respectively.

Fig. 5. Average dislocation densities on the $(111)[1\bar{1}0]$ slip system as a function of the gate length of the cells. Solid, broken and dashed lines denote the densities in the areas A, B and C, respectively.

Table.1 Dimensions of the models in unit of nm.

	w	h	d	L_g	t
Model 1	1140	1500	200	140	300
Model 2	741	1500	200	91	300
Model 3	228	461.5	61.5	28	92.3

Table.2 Material data for SiO_2 and Si.

Material	Elastic compliances $[10^{-11}\ m^2/N]$		
SiO_2	S_{11}=1.3698	S_{12}=-0.2327	S_{44}=3.2051
Si	S_{11}=0.7685	S_{12}=-0.2139	S_{44}=1.2563

Material	Lattice friction	Thermal expansion coefficient
SiO_2	10.0×10^3 [MPa]	0.35×10^{-6} [1/K]
Si	30.0 [MPa]	2.50×10^{-6} [1/K]

Table.3 The slip systems on which dislocations accumulate.

No.	Slip plane normal direction	Slip direction
1	(111)	$[1\bar{1}0]$
3	(111)	$[10\bar{1}]$
4	$(\bar{1}11)$	[110]
6	$(\bar{1}11)$	[101]
8	$(11\bar{1})$	[011]
1 1	$(1\bar{1}1)$	[011]

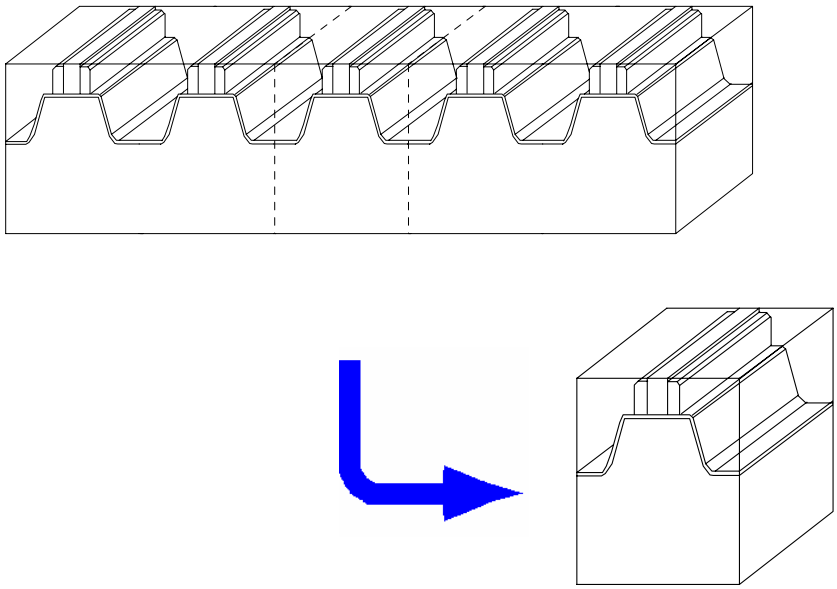

Fig. 1. Schematic illustration of the periodic structure of the STI type ULSI cells. One unit of the periodic structure is used for the analysis.

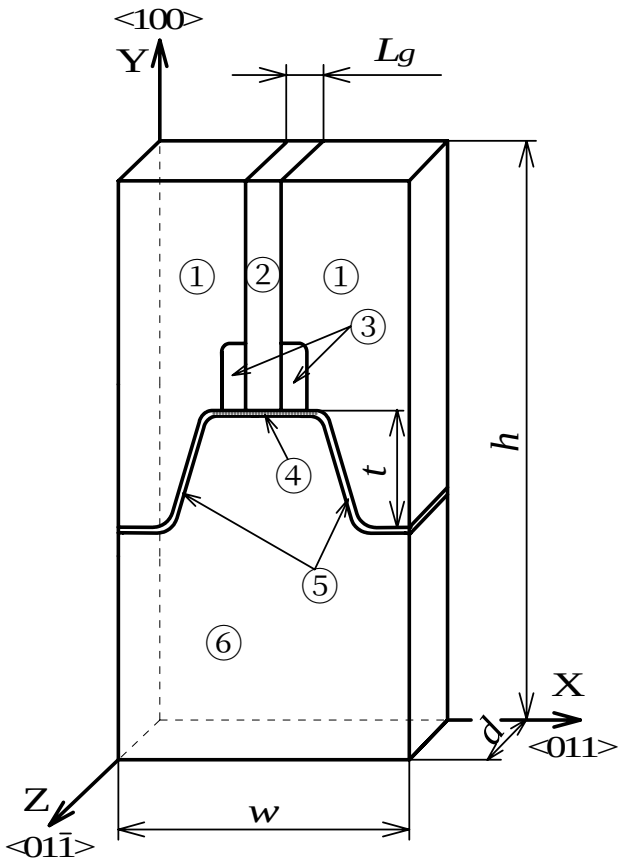

Fig. 2. Model employed for the crystal plasticity analysis. Volumes ① to ③ correspond to buried oxide, gate electrode, and source/drain electrodes, respectively. Volumes ④ and ⑤ correspond to the film region where dilatational transformation take place due to oxidation, and volume ⑥ represents the Si substrate, respectively. Crystal orientation of <011>, <100> and $<01\bar{1}>$ correspond to x, y and z axis, respectively.

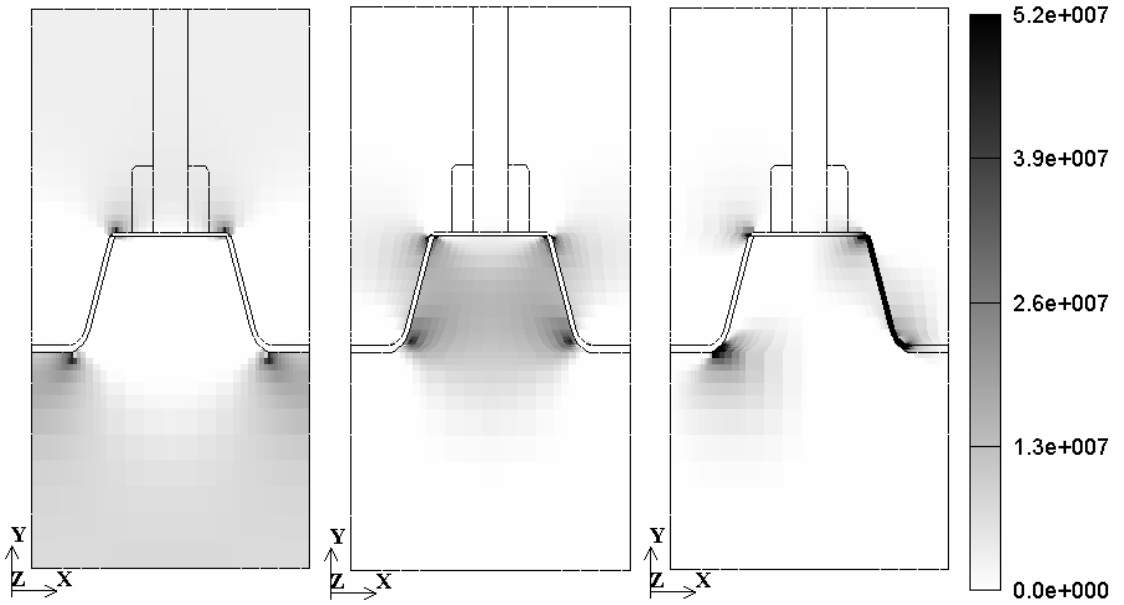

σ_{xx} σ_{yy} σ_{xy} Pa

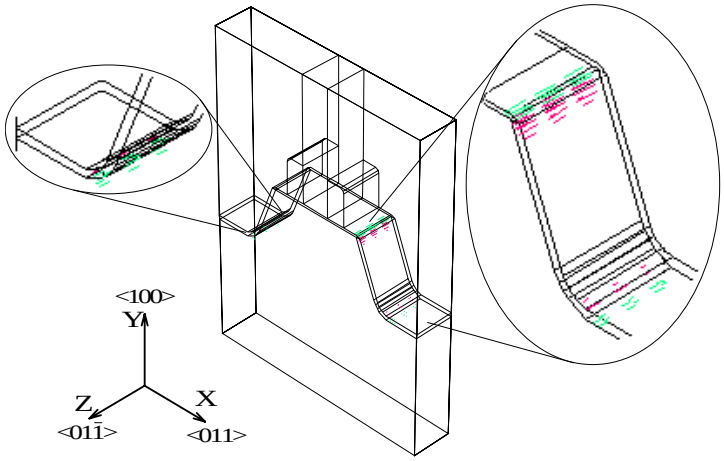

(a) Model 1

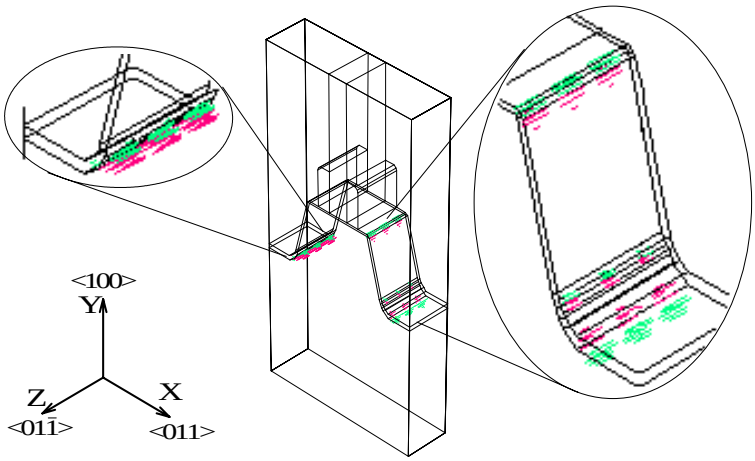

(b) Model 2

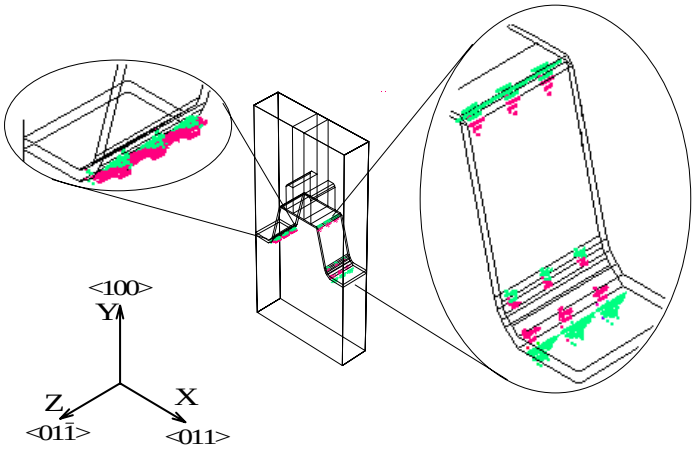

(c) Model 3

Fig.3 Numerical result for dislocations which accumulate on the $(111)[1\bar{1}0]$ slip system.

Longer and thicker line segments represent higher density of dislocations.

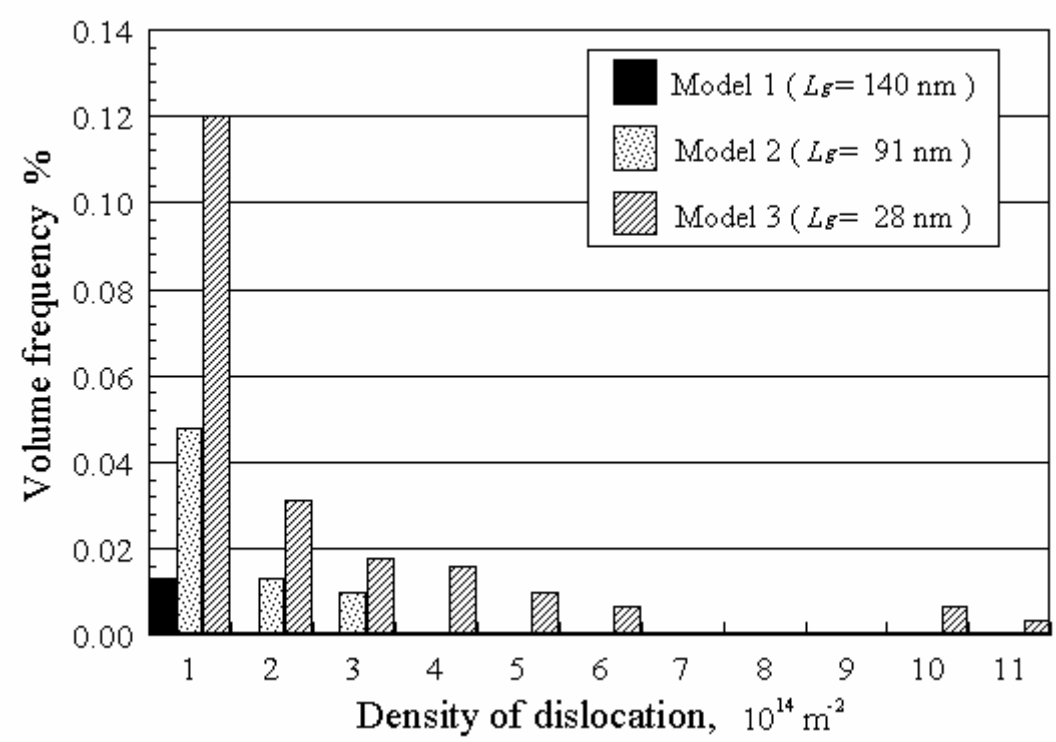

Fig.4 Volume frequency distribution of finite elements where dislocation density is larger than 1.0×10^{14} m^{-2}. The maximum dislocation densities in the model 1, 2 and 3 are 1.3×10^{14} m^{-2}, 3.2×10^{14} m^{-2} and 1.1×10^{15} m^{-2}, respectively.

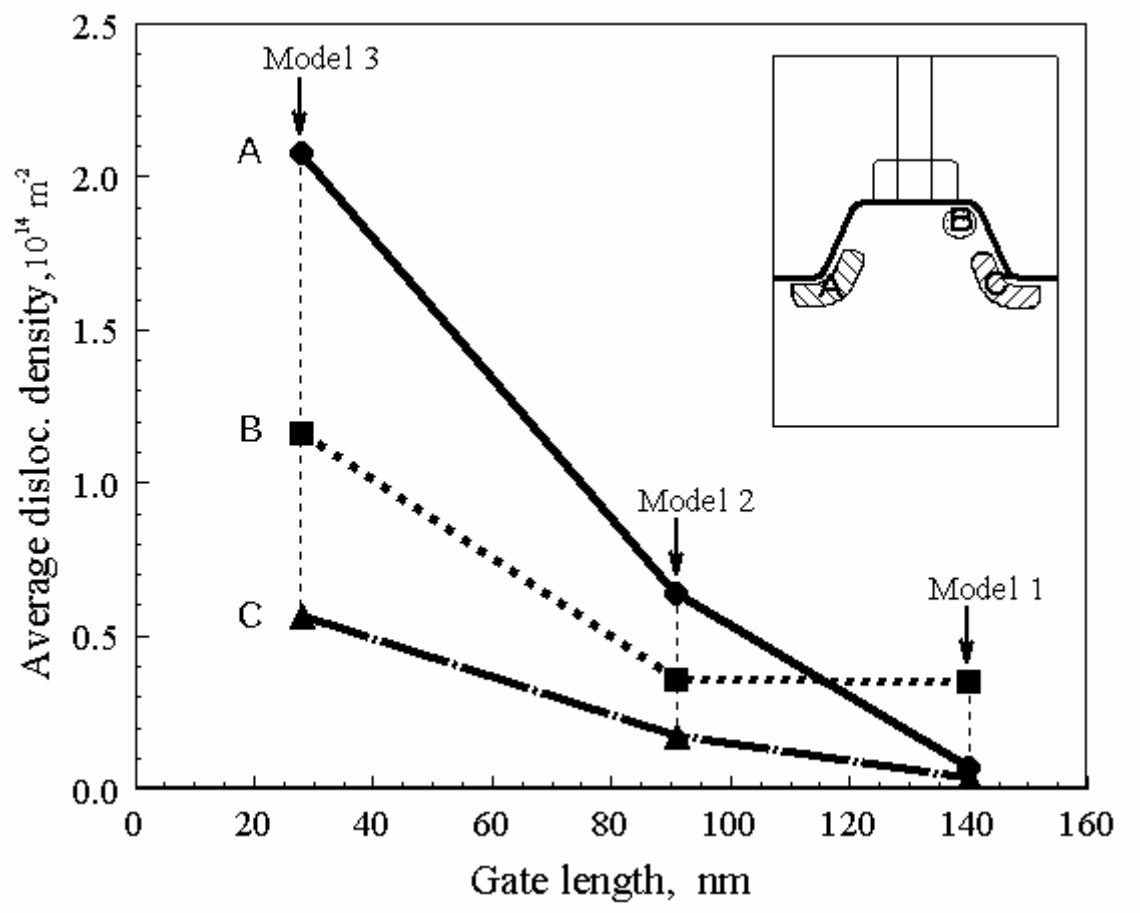

Fig.5 Average dislocation densities on the $(111)[1\bar{1}0]$ slip system as a function of the gate length of the cells. Solid, broken and dashed lines denote the densities in the areas A, B and C, respectively.